Available online at www.sciencedirect.com
ScienceDirect
Mendeleev Commun., 2013, **23**, 358–360
Mendeleev Communications

Cellular combustion at the transition of a spherical flame front to a flat front at the initiated ignition of methane–air, methane–oxygen and *n*-pentane–air mixtures

Ideya M. Naboko,[a] Nikolai M. Rubtsov,*[b] Boris S. Seplyarskii,[b] Kirill Ya. Troshin,[c] Georgii I. Tsvetkov[b] and Victor I. Chernysh[b]

[a] *Joint Institute for High Temperatures, Russian Academy of Sciences, 125412 Moscow, Russian Federation. E-mail: idnaboko@yandex.ru*
[b] *Institute of Structural Makrokinetics and Materials Science, Russian Academy of Sciences, 142432 Chernogolovka, Moscow Region, Russian Federation. Fax: +7 495 962 8025; e-mail: nmrubtss@mail.ru*
[c] *N. N. Semenov Institute of Chemical Physics, Russian Academy of Sciences, 119991 Moscow, Russian Federation*

DOI: 10.1016/j.mencom.2013.11.020

High-speed cinematography was used to study the transition of a spherical flame front to a flat front in *n*-pentane–air and methane–air mixtures initiated by a spark discharge. Cellular flame structures were observed at the transition. Modeling based on compressible reactive Navier–Stokes equations at a low Mach number showed a qualitative agreement with experimental data.

The majority of studies of gas-phase combustion processes are devoted to a stationary flame front (FF).[1–3] Actually, combustion occurs under conditions of non-stationary flows, density and pressure fluctuations; a flat flame is hydrodynamically unstable.[4] In nonstoichiometric mixtures, thermal diffusive instability is caused by the selective diffusion of a missing component. Joint action of thermal diffusive and hydrodynamic instabilities was studied.[5–9] Direct verification of a hypothesis[4] was undertaken.[10] As the flame instability area is displaced with variation of acoustic amplitude, a flat flame[10] was stabilized by an external acoustic field. Then, at shutdown of the field the growth rate of cellular structures on flat flame boundary was directly measured; the interrelation[10] of the hydrodynamic and acoustic flame instabilities[11] was illustrated.

In this work, stoichiometric fuel–oxygen mixtures, in which thermal diffusion does not play an essential role, were investigated. The fluctuations of the rate of heat release in time can be a source of acoustic perturbations;[10,11] thus, near combustion limits the probability of fluctuations of heat release is higher.[12] In spherical FF, perturbations develop more slowly than in a flat flame because the surface of spherical FF continuously grows.[1] However, after FF gets out of a spherical shape, for example, by transition along a cylindrical channel, hydrodynamic instability[4] can occur. In the experiment, the external stabilization of FF is not required because the initial spherical FF before contact with reactor walls is almost unperturbed.

Using the example of the combustion of stoichiometric *n*-pentane–air and lean methane–air mixtures, we studied the spatial distribution of FF under conditions when FF gets out of a spherical shape and displays hydrodynamic and acoustic instabilities of flat FF. For this purpose, the spatial distribution of FF of stoichiometric *n*-pentane–air, methane–oxygen mixtures diluted with an inert gas and lean methane–air mixes at 298 K and 1 atm in constant-volume reactors were investigated by means of colour high-speed cinematography.

The experiments were performed in a stainless steel cylindrical reactor (reactor *1*) 12 cm in diameter and 25 cm long supplied with an optical quartz window at butt-end [Figure S1(*a*), Online Supplementary Materials].[13,14] Spark electrodes were placed at the reactor centre. At 'side view' flame visualization a horizontally located quartz cylindrical reactor (reactor *2*) 70 cm in length and 14 cm in diameter [Figure S1(*b*)] was used.[15] The reactor was fixed in two stainless steel gateways at butt-ends, supplied with gas inlets.[15] Two electrodes of spark ignition (1.5 J) were located at its centre. In the reactor, a 15.4% CH_4 + 30.8% O_2 + 46% CO_2 + + 7.8% Kr mixture was used at an initial pressure of 160 Torr.[†]

In Figure 1, the video frames of FF propagation in reactor *1* for various gas mixtures are presented. First, an ignition centre[13–16] is registered, and then stationary FF propagation until a contact with reactor surface is observed. Just before the contact, the visible FF velocity decreases and FF is deformed near the openings of gas inlets. Further FF propagation occurs in a cylindrical part of reactor *1* to the butt-end from which filming is carried out. Injection of gas from the inlets into combustion products [Figure 1(*a*),(*c*),(*d*)] is accompanied by acoustic fluctuations in the reactor [Figure 1(*b*)]. As can be seen in Figure 1(*c*),(*d*), spherical FF is not actually perturbed[1] [Figure 1(*c*), shots 54–63]. Then, at propagation along reactor *1*, an unstable flat flame occurs as the theory[4] predicts, which is shown in the development of FF instabilities in the form of regular structures of combustion cells [Figure 1(*c*), shots 130–150; Figure 1(*d*), shots 100–130]. The cells on FF are characteristic of certain extent of inert gas dilution – in fast-burning (undiluted and poorly diluted) mixtures, the cells do not occur. With an increase in the extent of dilution, cell structures do not move [Figure 1(*a*)]; then, these flame structures containing hot combustion products move upward due to gravity forces [Figure 1(*c*),(*d*), see also Figure S2 and S3[16]]. Therefore, at dilution the probability of FF instabilities occurrence near combustion limits increases in agreement with published data.[12] By the time

[†] CO_2 was added for the reduction of FF velocity to improve the quality of video filming. Kr was added to reduce an initiation threshold for spark discharge. Speed filming of ignition dynamics and FF propagation was carried out from the butt-end [Figure S1(*a*)] or from the side of the reactor [Figure S1(*b*)] by means of a Casio Exilim F1 Pro colour high-speed digital camera (frames frequency, 60–1200 s^{-1}). The video file was stored in computer memory and its time-lapse processing was performed. The pressure change in the course of combustion was recorded by means of a piezoelectric gage synchronized with the discharge. Gases were chemically pure.

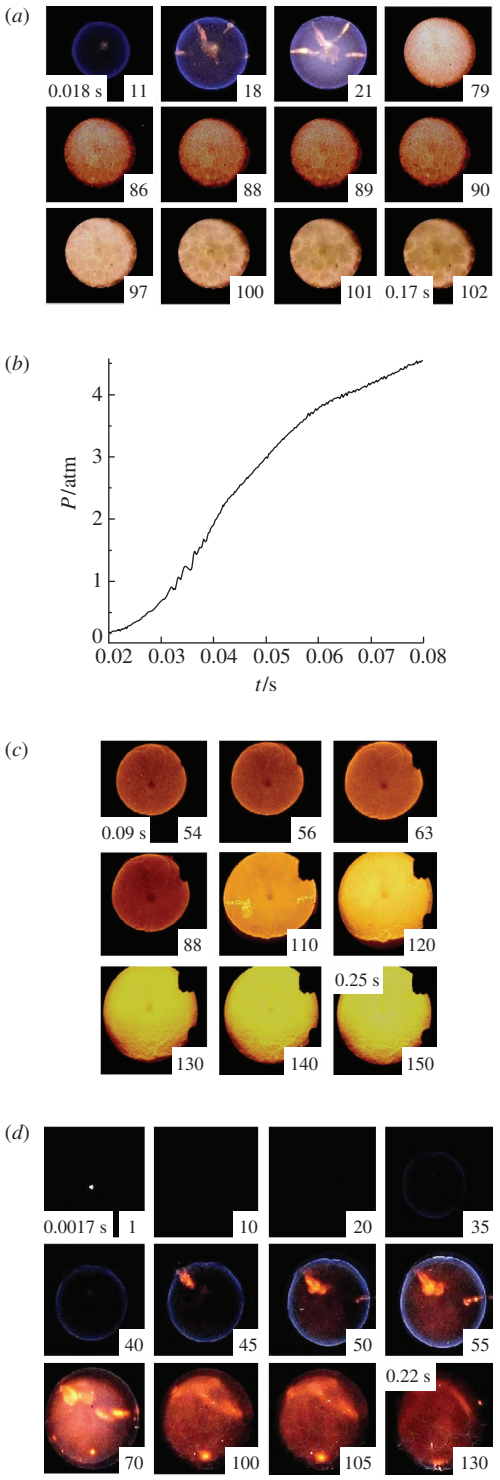

Figure 1 High-speed filming of FF in reactor *1*, 600 frames s^{-1}, the figure on a frame corresponds to frame number after discharge. (*a*) 80% $(C_5H_{12}$ + + air$)_{stoich}$ + 20% Ar. (*b*) Dependence of excess of total pressure over atmospheric on time under conditions of Figure S2. (*c*) 6.3% CH_4 + air, (*d*) 70% $(C_5H_{12}$ + air$)_{stoich}$ + 30% Ar.

of FF contact with the reactor butt-end, a regular cellular FF structure is observed.

The qualitative consideration of the transition of FF propagation from a spherical shape to a cylindrical one was performed by the solution of a two-dimensional problem in 'side view' projection to establish further ways of modification of numerical calculations. Both FF interaction with the reactor butt-end and FF transition from a circular shape to propagation in a flat channel at local initiation were considered. As is well known,[10,17,18] the interrelation of hydrodynamic and acoustic instabilities can be analyzed on the basis of compressible reactive Navier–Stokes equations at a low Mach number (that corresponds to subsonic combustion).‡ As is seen in Figure 1, cells on FF are registered by flame emission; therefore, an exothermic chemical reaction accompanied by energy release and temperature change proceeds in the cells. In Figure S2 (see Online Supplementary Materials),

‡ Compressible dimensionless reactive Navier–Stokes equations in low Mach number approximation were suggested.[17,21–24] The indexes t, x, y mean differentiation on t, x, y.

$$\rho T = P, \tag{1a}$$

$$\rho_t + (\rho v)_y + (pu)_x = 0, \tag{1b}$$

$$\rho(u_t + vv_y + uv_x) + P_y/\gamma M^2 = 1/\mathrm{Fr} + \mathrm{Sc}(\nabla^2 v + 1/3K_y) \tag{1c}$$

$$\rho(v_t + vu_y + uu_x) + P_x/\gamma M^2 = 1/\mathrm{Fr} + \mathrm{Sc}(\nabla^2 u + 1/3K_x) \tag{1d}$$

$$\rho(T_t + vT_y + uT_x) - (\gamma - 1)/\gamma P_t - (\gamma - 1)M^2(P_t + uP_x + vP_y) = = \nabla^2 T + \beta_1 W, \tag{1e}$$

$$\rho(C_t + vC_y + uC_x) = \nabla^2 C + \beta W, \tag{1f}$$

$$W = (1 - C)\exp(\zeta - \zeta/T), \tag{1g}$$

$$P_{tt} - 1/M^2\nabla^2 P = q(C_P - 1)\beta_1 W_t, \tag{1h}$$

where $\nabla^2 = (...)_{yy} + (...)_{xx}$ is the two-dimensional Laplace operator, $K = v_y + u_x$ is the viscous dissipation, $P_{tt} = \mathrm{d}^2P/\mathrm{d}t^2$, $\mathrm{d}(...)/\mathrm{d}t$ is a material derivative, u, v are the velocity components in the directions x, y, respectively, ρ is the density and T is the temperature; a chemical reaction is presented by a single first-order Arrhenius reaction, C is the reagent concentration, $1 - C$ is the extent of transformation, and ζ is a dimensionless coefficient. Dimensionless parameters: Schmidt's criterion $\mathrm{Sc} = \nu/D$, D is diffusivity (1 cm^2 s^{-1} at 1 atm[25]), ν is kinematic viscosity (10^{-5} cm^2 s^{-1}),[25] γ is the relation of constant pressure and constant volume thermal capacities; β_1 characterizes heat release allocation for concentration, β is kinetic coefficient. The initial values are the following: $\rho_0 = 0.001$ g cm^{-3}, $T_0 = 1$, $P_0 = \rho_0 T_0$, $\zeta = 10.5$, $\gamma = 1.4$, $\beta = 0.2$, $\beta_1 = 0.3$, $C_P = 0.3$ kal g^{-1} K^{-1} and $C_0 = 0.25$ Lewis's number is $\mathrm{Le} = 1$ that assumes the equality of $\mathrm{Sc} = \mathrm{Pr}$, where $\mathrm{Pr} = \rho_0 C_P \nu/\lambda$, λ is heat conductivity and C_P is thermal capacity at constant pressure. Scales of length and speed are determined as $l_\mathrm{d}^2 = Dt_\mathrm{d}$, and $U_d = l_\mathrm{d}/t_\mathrm{d}$, respectively. Reynolds's number is $l_\mathrm{d}U_\mathrm{d}/\nu = 1/\mathrm{Sc}$. Froude's number is $\mathrm{Fr} = U_\mathrm{d}^2/gl_\mathrm{d}$ (g is the acceleration of a free fall) accepted equal to 0.07. Mach number is $M = U_\mathrm{d}/c_0$ and it is accepted equal to 0.025, where c_0 is the speed of sound. It is obvious if $M = 0$, fluctuations of pressure are absent. At $M \to 0$, the reference value of average pressure of P_0 becomes much higher than the average value of $\rho_0 U_\mathrm{d}^2$ for pressure fluctuations at the average pressure P_0. The velocity field is determined by these fluctuations. If a standard representation of pressure is used, the usual replacement of variables $P = P_0 p$ leads to the occurrence of a factor $1/M^2$ in the term grad p in the impulse equation.[17,24] It is accepted that pressure values satisfy a wave equation (1h), which can be obtained from the continuity and impulse equations taking into account internal power sources and neglecting terms of order $1/M^4$.[11,26–28] Equation (1h), describing waves in the moving nonuniform media with a heat source, follows from continuity and impulse conservation equations [$q = l_\mathrm{d}^2/(U_\mathrm{d}^4\rho_0)$ – the parameter arising at reduction to dimensionless form]; therefore, set (1) is overdefined. To provide correspondence of the quantity of the equations with the number of unknowns, equation (1a) is excluded from set (1) in the further analysis.

In a number of calculations, the reaction velocity was presented by an elementary chain mechanism: $C \to 2n(w_0)$ and $n + C \to 2n +$ products. In this case, the equations (1f), (1g) were replaced with the following ones (initial condition for concentration changes to $C_0 = 1$).

$$\rho(C_t + vC_y + uC_x) = \nabla^2 C - \beta nW,$$

$$\rho(n_t + vn_y + un_x) = \nabla^2 n + 2\beta nW,$$

$$W = C\exp(\zeta - \zeta/T).$$

The solution of the problem was carried out by finite element analysis by means of the package (FlexPDE 6.08, A Flexible Solution System for Partial Differential equations, 1996-2008 PDE Solutions Inc.[29]). Initiation condition was taken $T = 10$ on the left boundary of the channel (Figure S2), or an impulse $T = 10$ in the geometrical centre of the channel (Figure S3). Boundary conditions were $C_x = 0$, $C_y = 0$, $n = 0$, as well as a convective heat exchange $T_t = T - T_0$, $u = 0$, $v = 0$, $\rho_x = 0$, $\rho_y = 0$.

the results of qualitative calculations of a temperature field at FF interaction with reactor butt-end in flat channel are presented. For reduction of calculation time the initiation by a whole opposite butt-end is set. After initiation, the stationary FF propagates from left to right (Figure S2). When FF reaches the right reactor butt-end, temperature instabilities occur, which move symmetrically to the channel axis at zero gravity. Under gravity conditions FF at first reaches the 'top' part of the channel and only then moves to its 'bottom' part; *i.e.*, temperature nonuniformities move 'downward' in a qualitative agreement with experimental data [*cf.* Figure 1(*c*),(*d*)]. Figure S2 allowed us to conclude that, if flame is fast enough that gravity does not affect FF propagation (*i.e.*, formally, $g = 0$), one must observe a motionless cell structure. It also qualitatively agrees with the experiment [Figure 1(*a*)]. Analysis of combustion kinetics set by the chain mechanism gives the same qualitative results as in Figure S2, but at $\zeta = 7$, *i.e.*, in agreement with published data,[19,20] the effective activation energy of the chain process is less than that of a single chemical reaction described by Arrhenius law.

The results of numerical modeling of a temperature field, along with the 'side view' filming of FF propagation in 15.4% CH_4 + + 30.8% O_2 + 46% CO_2 + 7.8% Kr, are presented in Figure S3 (see Online Supplementary Materials). The qualitative agreement with experimental results is observed. On calculated shots corresponding to experimental shots (2–8), FF nonuniformities occur upon transition from spherical FF to a flat flame. On calculated shot corresponding to experimental shot 14, the formation of regular structures on FF near the reactor wall is observed. In the experiment, FF velocity is high enough, and the influence of gravity is not essential.

Note that the analysis of a three-dimensional model is necessary for the description of quantitative regularities of the formation of regular structures on FF. At the same time, the results of the two-dimensional modeling are qualitatively consistent with the interpretation of FF cellular structure observed at the transition of a spherical flame front to a flat front in our experiments taking into account hydrodynamic and acoustic factors along with a chemical reaction.

The results obtained by the visualization of the development of flame front instabilities are important for the solution of explosion safety problems for volumes with complex geometry.

This work was supported in part by the Programme of Basic Research of the Presidium of the Russian Academy of Sciences (no. 26 'Combustion and Explosion').

Online Supplementary Materials

Supplementary data associated with this article can be found in the online version at doi:10.1016/j.mencom.2013.11.020.

References

1 Ya. B. Zel'dovich, G. A. Barenblatt, V. B. Librovich and D. V. Machviladze, *Matematicheskaya teoriya rasprostraneniya plameni (Mathematical Theory of Flame Propagation)*, Nauka, Moscow, 1980 (in Russian).
2 A. S. Sokolik, *Samovosplamenenie, plamya i detonatsiya v gasakh (Self-ignition, Flame and Detonation in Gases)*, Academy of Sciences of the USSR, Moscow, 1960 (in Russian).
3 Ya. B. Zeldovich and G. I. Barenblatt, *Combust. Flame*, 1959, **3**, 61.
4 L. Landau, *Acta Phys.-Chim. USSR*, 1944, **19**, 77.
5 G. H. Markstein, *Nonsteady Flame Propagation*, Pergamon, New York, 1964.
6 G. I . Sivashinsky, *Acta Astronaut*., 1977, **4**, 1177.
7 P. Clavin and F. A. Williams, *J. Fluid Mech*., 1982, **116**, 251.
8 P. Pelcé and P. Clavin, *J. Fluid Mech*., 1982, **124**, 219.
9 P. Clavin and P. Garcia, *J. Méc. Théor. Appl*., 1983, **2**, 245.
10 C. Clanet and G. Searby, *Phys. Rev. Lett*., 1998, **27**, 3867.
11 J. F. van Kampen, *PhD Thesis*, University of Twente, Enschede, The Netherlands, 2006.
12 T. Lieuwen and B. T. Zinn, *Proc. Combust. Inst*., 1998, **27**, 1809.
13 N. M. Rubtsov, B. S. Seplyarskii, K. Ya. Troshin, V. I. Chernysh and G. I. Tsvetkov, *Mendeleev Commun*., 2011, **21**, 218.
14 N. M. Rubtsov, B. S. Seplyarskii, K. Ya. Troshin, G. I. Tsvetkov and V. I. Chernysh, *Mendeleev Commun*., 2011, **21**, 31.
15 I. M. Naboko, N. M. Rubtsov, B. S. Seplyarskii, V. I. Chernysh and G. I. Tsvetkov, *Mendeleev Commun*., 2013, **23**, 163.
16 http://www.chemphys.edu.ru/media/files/2011-12-23-001.pdf (in Russian).
17 T. Alasard, *Arch. Ration. Mech. Anal*., 2006, **180**, 1.
18 http://www.chemphys.edu.ru/media/files/2011-12-23-002.pdf (in Russian).
19 N. N. Semenov, *O nekotorykh problemakh khimicheskoi kinetiki i reaktsionnoi sposobnosti (On Some Problems of Chemical Kinetics and Reactivity)*, Academy of Sciences of the USSR, Moscow, 1958, p. 685 (in Russian).
20 V. Akkerman, V. Bychkov, A. Petchenko and L.-E. Eriksson, *Combust. Flame*, 2006, **145**, 675.
21 H.-O. Kreiss, *Commun. Pure Appl. Math*., 1980, **33**, 399.
22 F. A. Williams, *Combustion Theory*, 2nd edn., The Benjamin/Cummings Publishing Co., Menlo Park, CA, 1985.
23 A. V. Voronkov, E. A. Zemskov, E. P. Sychugova and A. G. Churbanov, *PHYSOR*, Seoul, Korea, 2002, p. 56.
24 A. Majda, *Equations for Low Mach Number Combustion*, Center of Pure and Applied Mathematics, University of California, Berkeley, 1982, PAM-112.
25 *Tablitsy fizicheskikh velichin (Tables of Physical Values)*, ed. I. K. Kikoin, Atomizdat, Moscow, 1976, p. 1007 (in Russian).
26 D. I. Abugov and V. M. Bobylev, *Teoriya i raschet raketnykh dvigatelei tverdogo topliva (Theory and Calculations of Solid Fuel Rocket Jets)*, Mashinostroenie, Moscow, 1987 (in Russian).
27 P. Clavin, *Annu. Rev. Fluid Mech.*, 1994, **26**, 321.
28 M. J. Lighthill, *Proc. Royal Soc. London, Ser. A*, 1954, **222**, 1148.
29 G. Backstrom, *Simple Fields of Physics by Finite Element Analysis*, GB Publishing, 2005.

Received: 4th July 2013; Com. 13/4151